IEEE Access
Multidisciplinary ⋮ Rapid Review ⋮ Open Access Journal

Received November 21, 2020, accepted December 7, 2020, date of publication December 10, 2020,
date of current version December 28, 2020.

Digital Object Identifier 10.1109/ACCESS.2020.3043818

Sub-Synchronous Resonance Damping Control Strategy for DFIG Wind Turbines

JAVIER SAMANES[1,2], (Member, IEEE), EUGENIO GUBIA[1,2], (Member, IEEE), JESUS LOPEZ[1,2], (Member, IEEE), AND ROLANDO BURGOS[3], (Member, IEEE)

[1]Department of Electrical, Electronic and Communications Engineering, Public University of Navarre (UPNA), 31006 Pamplona, Spain
[2]Institute of Smart Cities (ISC), Public University of Navarre (UPNA), 31006 Pamplona, Spain
[3]Center for Power Electronics Systems (CPES), The Bradley Department of Electrical and Computer Engineering, Virginia Tech, Blacksburg, VA 24060, USA

Corresponding author: Javier Samanes (javier.samanes@unavarra.es)

This work was supported by the Agencia Estatal de Investigacion (AEI) (Spanish State Research Agency) under Grant PID2019-110956RB-I00/AEI/10.13039 and Grant DPI-2016-80641-R.

ABSTRACT Doubly-fed induction generator (DFIG) wind turbines connected to capacitive series-compensated transmission lines are prone to exhibit oscillatory behavior. The phenomena is called sub-synchronous resonances (SSRs), as these oscillations occur at frequencies below the fundamental component. This paper first develops a modeling methodology for DFIG wind turbines, based on impedance matrices, that is applied to model a real wind farm where SSRs were reported. The stability analysis performed shows how the interaction between the grid-side converter and the rotor-side converter contribute to the instability of DFIG wind energy conversion systems connected to series compensated grids. With this model, we propose a simple sub-synchronous resonance control strategy based on an orthogonal proportional action applied to the rotor currents, and a variable gain in the PI controller adjusted as a function of the DFIG rotational speed. This control strategy depends only on the rotor currents, which are local and already measured variables in any DFIG wind turbine, and is implemented in the rotor side converter, so it does not imply an additional cost at wind farm or wind turbine level and can be applied to any DFIG wind energy conversion system (WECS). Additionally, it proves to be robust for any line impedance series compensation level, and it does not need real-time information concerning the grid at which the wind turbine is connected, or its parameters. A real case study is considered, where the sub-synchronous resonance damping strategy presented in this work is able to stabilize the system for every possible line impedance compensation level.

INDEX TERMS Doubly-fed induction generator (DFIG), sub-synchronous resonance (SSR), wind turbine, resonance damping, frequency response.

I. INTRODUCTION

Wind farms are located in areas with high wind speeds, that are frequently far from consumption centers. The existing long transmission lines often include capacitors in series to increase its transmission capacity and harvest wind power with low voltage drops. Moreover, series compensation avoids the additional cost of building new transmission lines. However, the line series compensator interacts with doubly-fed induction generator wind turbines, creating oscillation problems that can lead to instability [1]. This instability appears when the net resistance at low frequencies becomes negative, usually below the fundamental frequency, as it reflects the power converter control loops and the DFIG rotational speed [2]. This phenomenon, in which the grid, the DFIG generator and the power converters and their control loops are involved, is referred to as sub-synchronous resonance and can effectively limit grid integration of wind power into the grid.

Several SSR events involving DFIG wind farms and series compensated transmission lines have been reported in Texas [3], [4], Minnesota [5] and China [6]. For this reason, an important effort has been dedicated to modeling and analyzing SSR phenomena, for instance, to determine the nature of SSRs and the influence of the system parameters.

Inherited from power system stability studies, the dominant approach in the literature is based on the analysis of the system closed–loop eigenvalues [1], [6]–[13]. In these

The associate editor coordinating the review of this manuscript and approving it for publication was Jenny Mahoney.

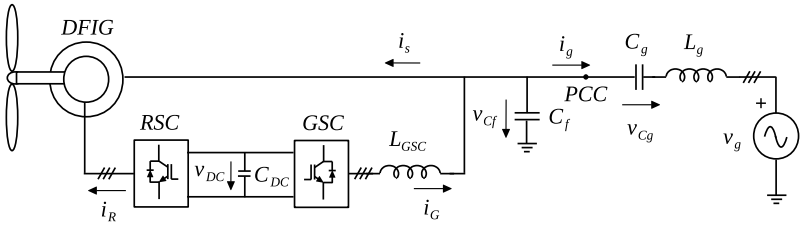

FIGURE 1. DFIG wind turbine with an *LCL* filter connected to a series compensated grid.

studies, a linear small–signal state–space model is derived. The eigenvalues of the resulting closed–loop state–space matrix are the system closed–loop poles. Following this methodology, participation factor studies and sensitivity analysis have concluded that the series compensation level, wind speed (rotational speed), and control loop gains, strongly influence the stability of DFIG wind turbines [1], [8]. Other modeling methodologies, commonly used by power electronic engineers, such as the impedance [14], [15] and complex vector modeling [16]–[18] have also been proposed to analyze SSRs. The model developed in this paper is based on transfer function matrices. Transfer function matrices can be systematically rotated between different reference frames [19], and can be used to model symmetric and non-symmetric MIMO systems without additional complexity, compared to complex transfer functions [20], [21]. Additionally, independent models can be developed and combined afterwards to build the complete model [22]. These models have a circuit representation, an interesting approach for power electronic engineers. Exploiting the benefits of transfer function matrices, in this paper a systematic modeling methodology is presented for DFIG wind turbines, which can be easily adapted for different wind turbine topologies and other case studies. This modeling methodology is combined with the frequency response analysis and its various tools, which have not been fully exploited, as the Bode diagram, for instance, that can help to understand the system dynamics and in the design of controllers and resonance damping control strategies [23].

To mitigate SSRs, the solutions proposed in the literature are focused on Flexible Alternating Current Transmission System (FACTS) [9], [24], [25], existing high-voltage direct-current (HVDC) links [26] and modifications of the DFIG control [7], [10]–[13], [17], [18], [27], [28]. This paper is focused in sub-synchronous resonance control strategies (SSRCS) implemented in the DFIG control, as FACTS imply an extra cost at wind farm or transmission level and HVDC are not always present in wind farms.

DFIG wind turbines include two power converters, the rotor side converter (RSC) and the grid side converter (GSC), as represented in Fig. 1. The control loops of both converters can be modified in order to damp SSRs and avoid instability. Some authors have proposed SSRCS for the GSC [7], [10], others for the RSC [11], [13], [17], [18] while others have combined damping strategies for both the RSC and the GSC [12], [27].

Concerning SSRCS implemented in the GSC, [7] and [10] demonstrated that an action proportional (P) to the voltage across the line compensation series capacitor, v_{Cg}, is an effective control signal for SSR damping, a finding shared by [12]. The voltage across the series capacitor is a remote signal, so they proposed estimators. Nevertheless, the accuracy of these estimators, and consequently the damping provided to the SSRs, can be compromised when the line compensation level varies or other generating units are connected to the same transmission line.

Overall, the RSC control loop parameters have a greater influence in the SSR phenomena, and thus, it is the preferred choice to damp sub-synchronous resonances, even if the stability of other modes can be compromised [7], [10]. [17] proposed a SSRCS based on complex gains adjusted using the Linear-Quadratic Regulator (LQR) theory. They also introduce an observer to align the *dq* axis with the grid voltage, v_g, instead of the stator voltage, in order to reduce oscillations at sub-synchronous frequencies. The accuracy of this estimator relies on the grid impedance parameter knowledge. [11] proposed a damping control strategy for the RSC, based on an action dependent of the stator, i_S, and rotor currents, i_R, and a state observer. The RSC damping strategy proved to be superior to a controller implemented in the GSC based on the modification of the reactive current reference. Nevertheless, the observer depends on the grid impedance parameters. As an alternative, a damping action can be implemented through a gain with phase compensation applied to the generated active power [13], filtered with a band-pass (BP) filter to act only in the desired range of frequencies. Even though the current dynamics are included in the active power, this variable has additional frequency components as a result of the interaction with the voltage. [18] presented a SSRCS based on the emulation of a virtual resistor in series with the stator winding and a virtual inductance in series with the rotor winding. With this purpose, they combine a proportional action filtered by a high-pass (HP) filter and a derivative action.

Other authors combined the actions of the GSC and the RSC to damp SSRs. [12] as mentioned previously, uses the estimated series capacitor voltage in the GSC and an additional derivative action in the RSC to emulate a virtual

TABLE 1. State of the art control strategies to mitigate sub-synchronous resonances.

Reference	Converter										External	Variable				Grid impedance knowledge	
	RSC					GSC						Local		Remote			
	Loop		Axis		Controller	Loop		Axis		Controller		Meas.	Est.	Meas.	Est.	Req.	Not req.
	Inner	Outer	d	q		Inner	Outer	d	q								
[7]							x	x	x	P					v_{Cg}	x	
[9]							x	x		P	x			v_{Cg}			x
[10]							x	x	x	P					v_{Cg}	x	
[11]	x		x	x	P + BP filter State observer							i_R, i_S				x		
[12]	x		x	x	Derivative		x		x	HP filter and P		i_R			v_{Cg}		x
[13]		x		x	P Lead-lag BP filter							Power					x
[17]	x		x	x	Complex P Observer							i_S, v_{Cf}			v_g	x	
[18]	x		x	x	P + HP filter Derivative							i_S					x
[27]	x		x		Notch		x	x		Notch		i_R, v_{DC}					x

inductance in series with the rotor winding. Lastly, [27] proposed the insertion of notch filters preferably in the DC-voltage, v_{DC}, control loop of the GSC or the inner current control loop of the RSC. However, if the line compensation level varies, the performance of the SSRCS can be compromised.

Table 1 summarizes the already described state of the art sub-synchronous resonance damping control strategies for the RSC and the GSC. Even though an important number of solutions exist, there are few that do not depend on remote measurements, or their estimation, which rely on the grid impedance knowledge. For this reason, this paper focuses on a novel damping strategy, based solely in local variables, robust, and applicable to any existing or new DFIG wind turbine, that guarantees the stability for any line impedance compensation level.

The control strategy proposed in this paper depends only on local and existent current measurements; namely the rotor currents, and programmed in the RSC. Accordingly, its implementation does not imply an extra cost and is applicable to any new or existing DFIG wind turbine. The proposed control strategy is derived after a detailed stability analysis, where the interaction between the GSC and RSC control loops reveals to be a key aspect that has to be considered to properly capture the unstable dynamics involved in sub-synchronous resonance phenomena. The system is modeled using transfer function matrices to capture cross-coupling dynamics, as DFIG wind turbines are normally controlled in the synchronous reference frame or *d-q* frame. A model for the phase-locked loop (PLL), using transfer function matrices is also developed to evaluate the PLL influence on the overall system stability. The stability of the derived MIMO model is analyzed by means of the Bode diagram and the MIMO Generalized Bode Criterion (MIMO GBC) [23]. This stability criterion is based on the open-loop frequency response analysis, different to the conventional approach in SSR literature focused on the closed–loop system eigenvalues. With the open-loop frequency response analysis, the identification of the unstable dynamics becomes more intuitive, specially for power electronic engineers who program the control loops of the RSC and the GSC. Thus, the identification of possible solutions and damping control strategies becomes easier.

II. SYSTEM MODELING AND STABILITY ANALYSIS

A. SYSTEM DESCRIPTION AND MODEL

In a DFIG wind turbine, as the one represented in Fig. 1, the RSC controls the torque and the rotational speed through a current control loop, while the GSC controls its output current to regulate the DC-bus voltage. Both GSC and RSC can be considered as two power converters connected in parallel to the grid, so both dynamics and control loops should be simultaneously considered to properly study the system stability.

In this subsection the plant physical model is obtained for the DFIG wind energy conversion system. Independent models for the DFIG, the harmonic *LC* filter and the grid are obtained, which are later combined to build the complete plant model that considers the influence of the GSC on the RSC and vice-versa. The grid inductance, L_g in Fig. 1, includes the grid and transformer leakage inductances.

DFIG wind turbines are normally controlled in the synchronous reference frame or *d-q* axis, so all the elements are modeled in this frame. Impedance matrices are used to model the different components, as they are a straightforward approach to model the cross-coupling terms between both axis. Moreover, this modeling methodology can be used for symmetric and non-symmetric systems [20], [23], as the ones obtained when the power control loops and the PLL effect cannot be neglected for the stability analysis.

In this paper 2×2 matrices are denoted between brackets, while vectors are denoted by capital letters with the subscript *dq* to indicate the reference frame in which they are expressed. The subindex outside the matrix brackets specifies the angular speed of the cross-coupling terms.

1) DFIG MODEL

With the notation presented, the equations of a doubly-fed induction generator can be compactly expressed as:

$$V_{Sdq} = [Z_{L_m}]_{\omega_0} I_{Rdq} + [Z_{RL_S}]_{\omega_0} I_{Sdq} \quad (1)$$

$$V_{Rdq} = [Z_{RL_R}]_{\omega_R} I_{Rdq} + [Z_{L_m}]_{\omega_R} I_{Sdq}, \quad (2)$$

where the subscripts R and S specify whether the current, I or voltage V, belong to the rotor or stator terminals. ω_0 is the rotational speed of the d-q axis, synchronized with the grid voltage, and $\omega_R = \omega_0 - \omega_m$, ω_m being the rotor electrical rotational speed. The matrices $[Z_{L_m}]_\omega$, $[Z_{RL_S}]_{\omega_0}$ and $[Z_{RL_R}]_{\omega_R}$ are provided by:

$$[Z_{L_m}]_\omega = \begin{bmatrix} L_m s & -L_m \omega \\ L_m \omega & L_m s \end{bmatrix} \quad (3)$$

$$[Z_{RL_S}]_{\omega_0} = \begin{bmatrix} R_S + L_S s & -L_S \omega_0 \\ L_S \omega_0 & R_S + L_S s \end{bmatrix} \quad (4)$$

$$[Z_{RL_R}]_{\omega_R} = \begin{bmatrix} R_R + L_R s & -L_R \omega_R \\ L_R \omega_R & R_R + L_R s \end{bmatrix} \quad (5)$$

where R_R and R_S are the winding series resistance, L_m the magnetizing inductance, L_S equals the sum of L_m and the stator leakage inductance and L_R the sum of L_m and the rotor leakage inductance. All the parameters in the DFIG model are referred to the stator. Note as well that the impedance $[Z_{L_m}]_\omega$ is evaluated at ω_R and ω_0 in (1) and (2). Both equations can be rearranged, to express the currents as a function of the voltages at the rotor and stator terminals

$$I_{Sdq} = [Y_{I_S V_R}] V_{Rdq} + [Y_{I_S V_S}] V_{Sdq}, \quad (6)$$

$$I_{Rdq} = [Y_{I_R V_R}] V_{Rdq} + [Y_{I_R V_S}] V_{Sdq} \quad (7)$$

where

$$[Y_{I_S V_R}] = \left([Z_{L_m}]_{\omega_R} - [Z_{RL_R}]_{\omega_R} [Z_{L_m}]_{\omega_0}^{-1} [Z_{RL_S}]_{\omega_0} \right)^{-1}, \quad (8)$$

$$[Y_{I_S V_S}] = -[Y_{I_S V_R}] [Z_{RL_R}]_{\omega_R} [Z_{L_m}]_{\omega_0}^{-1}, \quad (9)$$

$$[Y_{I_R V_R}] = [Z_{L_m}]_{\omega_0}^{-1} [Z_{RL_S}]_{\omega_0} [Y_{I_S V_R}], \quad (10)$$

and

$$[Y_{I_R V_S}] = [Z_{L_m}]_{\omega_0}^{-1} \left([I_2] - [Z_{RL_S}]_{\omega_0} [Y_{I_S V_S}] \right). \quad (11)$$

$[I_2]$ is the order two identity matrix. According to Fig. 1, the stator voltage equals the LC capacitor voltage

$$V_{Sdq} = V_{Cfdq}. \quad (12)$$

2) HARMONIC LC FILTER MODEL

As represented in Fig. 1 the GSC is connected to the stator terminals through an inductor, L_{GSC}, and to the grid by parallel capacitors, C_f, to form an LC filter. The inductor is modeled by a matrix impedance $[Z_{RL_G}]_{\omega_0}$, as in (4), with a series resistance R_{GSC} and an inductance L_{GSC}. The current across the inductor, I_{Gdq}, is

$$I_{Gdq} = [Z_{RL_G}]_{\omega_0}^{-1} \left(V_{Gdq} - V_{Cfdq} \right), \quad (13)$$

where V_{Gdq} is the voltage imposed by the GSC. The filter capacitance, C_f, has a series damping resistance, R_d, and its impedance, $[Z_{Cf}]_{\omega_0}$, is given by

$$[Z_{Cf}]_{\omega_0} = \begin{bmatrix} R_d + \dfrac{s}{C_f(s^2+\omega_0^2)} & \dfrac{\omega_0}{C_f(s^2+\omega_0^2)} \\ -\dfrac{\omega_0}{C_f(s^2+\omega_0^2)} & R_d + \dfrac{s}{C_f(s^2+\omega_0^2)} \end{bmatrix}, \quad (14)$$

and

$$V_{Cfdq} = [Z_{Cf}]_{\omega_0} I_{Cfdq}. \quad (15)$$

3) GRID MODEL

The grid voltage does not have an influence on the stability, and consequently it is neglected in this analysis. In such way, the grid current I_{gdq} is related to V_{Cfdq} by

$$V_{Cfdq} = [Z_g]_{\omega_0} I_{gdq}, \quad (16)$$

where

$$[Z_g]_{\omega_0} = \begin{bmatrix} R_g + L_g s + \dfrac{s}{C_g(s^2+\omega_0^2)} & -L_g \omega_0 + \dfrac{\omega_0}{C_g(s^2+\omega_0^2)} \\ L_g \omega_0 - \dfrac{\omega_0}{C_g(s^2+\omega_0^2)} & R_g + L_g s + \dfrac{s}{C_g(s^2+\omega_0^2)} \end{bmatrix} \quad (17)$$

The grid impedance is formed by a series resistor, R_g, the series compensation capacitance, C_g, and the grid equivalent inductance, L_g. L_g models the leakage inductance of the step-up transformer within the nacelle, park and distribution transformers, as well as the transmission line distributed inductance. It should be noted that a wind farm is formed by several equal wind turbines connected in parallel at the point of common coupling (PCC), so the method presented in [29] to aggregate generation units is used.

4) PLANT MODEL

(6), (7), (12), (13), (15) and (16) can be combined with

$$I_{Gdq} = I_{Sdq} + I_{Cfdq} + I_{gdq} \quad (18)$$

to derive the plant model that takes into consideration the interaction between the GSC and RSC. The goal is to determine the relation between the currents to be controlled, I_{Gdq} and I_{Rdq}, and the input voltages, V_{Gdq} and V_{Rdq}, given by

$$I_{Gdq} = [P_{I_G V_G}] V_{Gdq} + [P_{I_G V_R}] V_{Rdq} \quad (19)$$

$$I_{Rdq} = [P_{I_R V_G}] V_{Gdq} + [P_{I_R V_R}] V_{Rdq}. \quad (20)$$

The expressions for $[P_{I_G V_G}]$, $[P_{I_G V_R}]$, $[P_{I_R V_G}]$ and $[P_{I_R V_R}]$, are provided in Appendix A by (30)-(33).

B. RSC AND GSC CONTROL

The RSC and the GSC are controlled as current sources, assuming that the grid is a voltage source. The block diagram of the current control loop of each power converter appears in Fig. 2, showing that their dynamics are coupled. Both converter output currents are controlled in the d-q frame using a PI regulator. The measured currents are filtered by

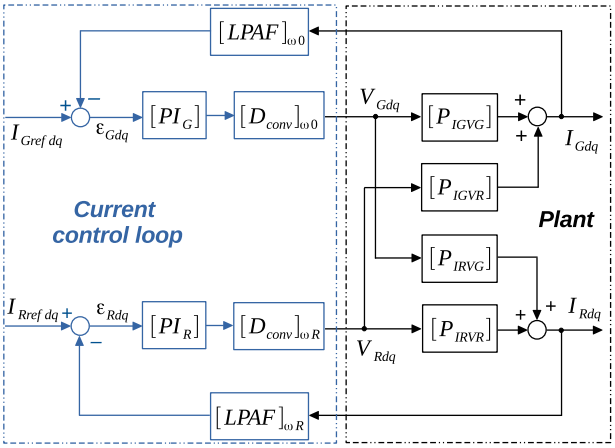

FIGURE 2. RSC and GSC current control loops.

a low pass-pass analog filter, $LPAF = 1/(\tau s + 1)$, while the block D_{conv} models the delay of one sample time, introduced by the computation in the DSP, and the effect of the zero order hold, that represents the PWM power converter. A forth order approximation is used for D_{conv}, in order to achieve an accurate representation [22].

In a DFIG wind turbine controlled in the synchronous reference frame, there are three different reference frames where the control elements are defined. The grid-side converter $LPAF$, as well as the ZOH and computational delay, are defined in the stator stationary reference frame, $\alpha\beta_s$. The rotor-side converter $LPAF$ and the ZOH and computational delay are defined in a stationary reference frame rotating with the rotor windings at ω_m, $\alpha\beta_m$. At last, both PI controllers are defined in the synchronous reference frame or d-q coordinates.

As previously mentioned, the system stability is analyzed in the synchronous reference frame, synchronized with the grid voltage frequency, ω_0, so all the elements must be transformed to this frame. The transformation presented in [19] is used to rotate the transfer functions between the different frames. For instance, lets consider the $LPAF$ defined in a stationary reference frame, its equivalent model in d-q axis is a 2×2 MIMO model

$$[LPAF]_\omega = \frac{1}{2}\begin{bmatrix} LPAF_1(s) & LPAF_2(s) \\ -LPAF_2(s) & LPAF_1(s) \end{bmatrix}, \tag{21}$$

where $LPAF_1(s) = LPAF(s + j\omega) + LPAF(s - j\omega)$ and $LPAF_2(s) = jLPAF(s + j\omega) - jLPAF(s - j\omega)$. The $LPAF$ in the GSC and the RSC have the same time constant, τ, but the resulting models in d-q axis are different, as each element is rotated with a different speed. For the GSC, as the $LPAF$ is defined in $\alpha\beta_S$, the rotation is made with ω_0, $[LPAF]_{\omega_0}$. In contrast, for the RSC, as the filter is defined in $\alpha\beta_m$, rotating at ω_m, the transformation is made with ω_R, $[LPAF]_{\omega_R}$. The same rotation is applied to D_{conv}, resulting in two different models for the GSC and the RSC, $[D_{conv}]_{\omega_0}$ and $[D_{conv}]_{\omega_R}$.

The last element in the current control loop is the PI controller, which is defined in d-q axis as a diagonal matrix

$$[PI] = \begin{bmatrix} K_p\dfrac{T_n s + 1}{T_n s} & 0 \\ 0 & K_p\dfrac{T_n s + 1}{T_n s} \end{bmatrix}. \tag{22}$$

The difference between $[PI_R]$ and $[PI_G]$ in Fig. 2 are the PI parameters, K_{pR} and T_{nR} for the RSC, and K_{pG} and T_{nG} for the GSC.

C. PLL MODEL

Grid-connected power converters require a synchronization with the grid voltage, normally made through a phase-locked loop, PLL. As the grid voltage cannot be measured, the voltage at the PCC, v_{Cf}, is used instead. This way, the PLL interacts with the current control loops, and can modify its dynamics at low frequencies, with an influence on the stability [20], [30]. As SSRs are a low frequency phenomena, the PLL has to be considered in the modeling procedure.

The PLL used in this paper is the one represented in Fig. 3. The capacitor voltage expressed in the stationary reference frame $\alpha\beta_S$ is filtered by a SOGI filter to extract the grid fundamental frequency component [31]. The capacitor voltage is aligned with the d axis, for this purpose a PI controller, PI_{PLL}, modifies the angular speed, ω_0, to drive V_q to zero. The resulting angle, θ_0, is fed to the Park transformation, $[P_T]$.

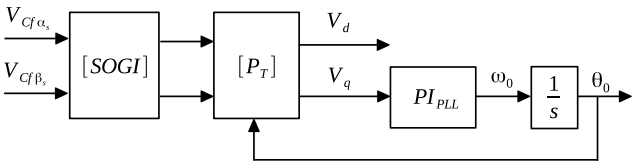

FIGURE 3. Phase-locked loop used for grid synchronization.

In Fig. 3 $[SOGI]$ is a diagonal matrix whose terms are equal to $FSOGI = k\omega s/(s^2 + k\omega s + \omega^2)$. This filter is applied to the $\alpha\beta_S$ components of the capacitor voltage, $V_{Cf\alpha\beta S}$, so it has to be rotated to d-q coordinates, obtaining a matrix as in (21), with $FSOGI_1 = FSOGI(s + j\omega) + FSOGI(s - j\omega)$ and $FSOGI_2 = jFSOGI(s + j\omega) - jFSOGI(s - j\omega)$.

With the modeling procedure presented in [20], the effect of the Park direct and inverse transformations used in the current control loops is represented as a disturbance dependent on the capacitor voltage. On the one hand, $[P_T]$ is applied to the GSC and the RSC currents. In the case of the rotor, the angle for the Park transformation equals $\theta_0 - \theta_m$, θ_m being the electrical angle measured by the rotor encoder. On the other hand, the inverse Park transformation is applied to the output of the PI voltage of both converters. The disturbances added to the current control loops are represented in green in Fig. 4. It can be seen that the plant includes two new blocks in order to obtain the capacitor voltage. The rotor current is multiplied by $[Z_{RLS}]_{\omega_0}^{-1}[Z_{L_m}]_{\omega_0}$ and added to I_{Gdq}, the result

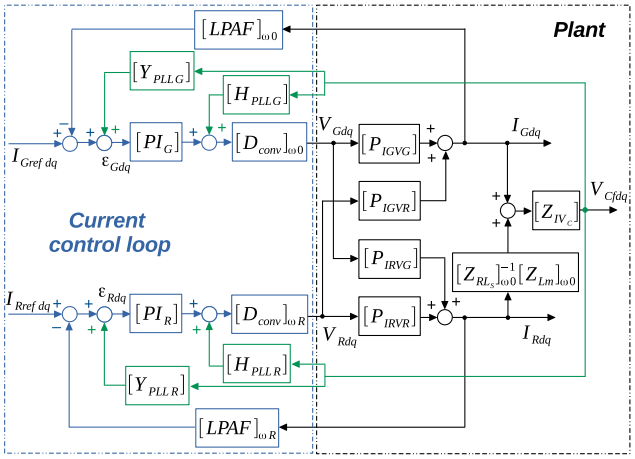

FIGURE 4. RSC and GSC current control loops including the PLL model.

is multiplied by the impedance

$$[Z_{IV_C}] = \left([Z_{RL_S}]^{-1}_{\omega_0} + [Z_{Cf}]^{-1}_{\omega_0} + [Z_g]^{-1}_{\omega_0}\right)^{-1}. \quad (23)$$

The transfer matrices $[H_{PLL}]$ and $[Y_{PLL}]$ in Fig. 4 are obtained through the PLL and the Park transformation linearization, and are equal to

$$[H_{PLL}] = \begin{bmatrix} 0 & -FT_{PLL}\overline{V_q} \\ 0 & FT_{PLL}\overline{V_d} \end{bmatrix}, \quad (24)$$

$$[Y_{PLL}] = \begin{bmatrix} 0 & -FT_{PLL}\overline{I_q} \\ 0 & FT_{PLL}\overline{I_d} \end{bmatrix}, \quad (25)$$

where

$$FT_{PLL} \approx \frac{PI_{PLL}FSOGI_1}{s + PI_{PLL}FSOGI_1\overline{V_{Cfd}}}. \quad (26)$$

$\overline{V_{Cfd}}$, $\overline{V_d}$, $\overline{V_q}$, $\overline{I_d}$ and $\overline{I_q}$ are the steady-state operating values for the voltages and currents. It should be noted that the matrices $[Y_{PLL}]$ and $[H_{PLL}]$ are different for the RSC and the GSC, as the steady-state currents, $\overline{I_{Gdq}}$ and $\overline{I_{Rdq}}$, are different in each converter, as well as the voltages imposed by each control loop, $\overline{V_{Gdq}}$ and $\overline{V_{Rdq}}$. In contrast, FT_{PLL} is the same as it only depends on the filter capacitor voltage in the d-axis, as the q-axis projection equals zero.

D. STABILITY ANALYSIS

To analyze the system stability, the MIMO Generalized Bode Criterion (MIMO GBC) is applied [23]. According to this criterion

$$Z = P - [2(C^+ - C^-) + C_0], \quad (27)$$

where Z is the number of closed-loop unstable poles and P is the number of open-loop unstable poles. C^+ and C^- are the $\pm m180$ degrees crossings with positive magnitude (m odd integer) counted in the Bode diagram of all the system open–loop eigenvalues only at positive frequencies. C^+ are the eigenvalue's positive crossings (with increasing phase), C^- the negative crossings (with decreasing phase) and C_0 are the crossings at 0 Hz.

As a case study to analyze the stability of DFIG wind turbines connected to series compensated grids and develop SSRCS, the parameters of a real SSR event reported in Texas are used [11], which are summarized in Appendix B.

According to the case study under consideration and the parameters provided, the short circuit ratio (SCR) at the PCC considering the wind farm substation and distribution grid impedance equals 5.5, without line impedance compensation. This is the case of a weak grid, and under weak grid conditions, the PLL can become a source of instability [20], [32]. Nevertheless, the PLL becomes a critical element for extreme weak grids, with SCR below 3.5. To evaluate whether the instability of DFIG wind turbines connected to series compensated grids is introduced by the PLL or is inherent to the current control loops, the stability analysis is performed first without the PLL, in the next subsection, and is included later to compare the results.

1) CURRENT CONTROL LOOP STABILITY WITHOUT THE PLL

The stability of the current control loops represented in Fig. 2 is first studied. The open-loop transfer matrix, $[H_{ol}]$, correlating the current and the error presents the following symmetry

$$\begin{Bmatrix} I_d \\ I_q \end{Bmatrix} = \begin{bmatrix} H_{ol1} & H_{ol2} \\ -H_{ol2} & H_{ol1} \end{bmatrix} \begin{Bmatrix} \varepsilon_d \\ \varepsilon_q \end{Bmatrix}, \quad (28)$$

which is the same symmetry found in the plant, as well as the current control loop matrices. The eigenvalues of symmetric matrices have the following simple expression

$$\lambda_{1,2} = H_{ol1} \pm jH_{ol2}. \quad (29)$$

The open-loop transfer matrices $[H_{Gol}]$ for the GSC current control loop and $[H_{Rol}]$ for the RSC one, are computed for a slip equal to 0.25. This means that the rotational speed of the DFIG is low, and under these circumstances the risk of SSRs increases [1]. As a first step, the interaction between the GSC and RSC control loops is neglected. This means that the open-loop transfer matrix $[H_{Gol}]$ is computed considering $V_{Rdq} = 0$, and $[H_{Rol}]$ computed for $V_{Gdq} = 0$. In Fig. 5 the eigenvalues' Bode diagram of $[H_{Rol}]$, $\lambda_{R1,2}$, are represented in blue, while the GSC ones, $\lambda_{G1,2}$, are represented in orange. Fig. 5 (a) shows that there are no ± 180 degree crossings with positive magnitude in none of the eigenvalues ($C^+ = C^- = 0$), neither for the GSC nor for the RSC. Moreover, as there are no open loop unstable poles ($P = 0$), both current controllers are stable when they do not interact with each other.

However, as already explained in the modeling subsection, both the RSC and GSC current control loops interact with each other. $[H_{Gol}]$ is recalculated, but this time considering the RSC closed-loop (with $I_{Rref\ dq} = 0$), and $[H_{Rol}]$ considering the GSC closed-loop (with $I_{Gref\ dq} = 0$). The eigenvalues of the resulting transfer function matrices are represented in Fig. 5 (b). In this case, λ_{R1} and λ_{G1} have

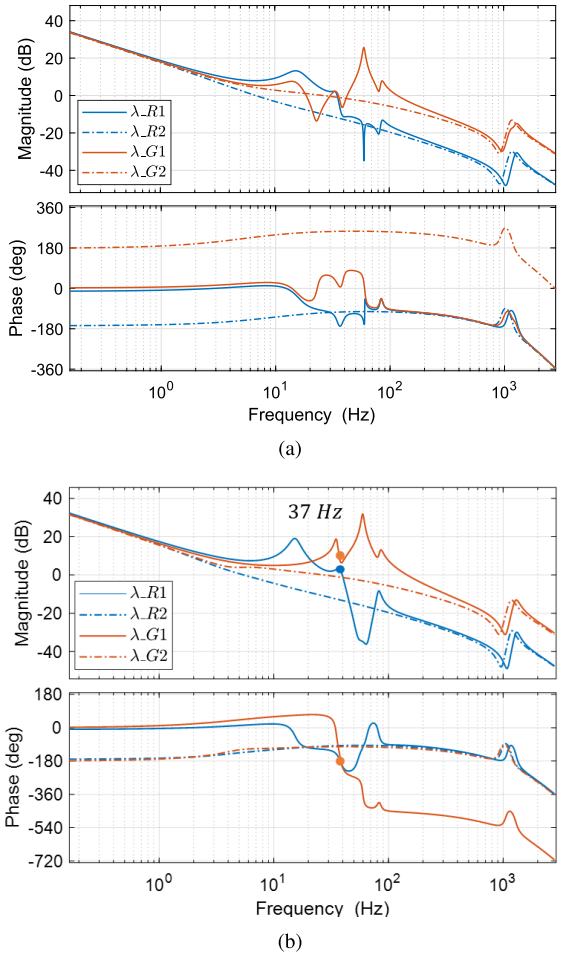

FIGURE 5. Eigenvalues' Bode diagrams for the RSC and GSC current control loops (a) neglecting, and (b) considering the interaction between the GSC and RSC.

a C^- crossing at 37 Hz, the equivalent SSR frequency in d-q coordinates. This means that both current control loops have two closed-loop unstable poles ($Z = 2$) according to (27), as $C_0 = C^+ = P = 0$.

It can be concluded from this preliminary stability analysis, that the interaction between the GSC and the RSC control loops needs to be considered to properly characterize SSR instabilities under series compensated grids, otherwise the model can neglect the underlying problem. Another important aspect is that the $\pm m180$ degree crossings in the eigenvalues' Bode diagram, for both the GSC and RSC, that lead to the closed-loop instability, occur only in one of the two eigenvalues.

The instability of DFIG wind turbines connected to series compensated grids occurs as a result of the coupled dynamics in $[H_{ol}]$, as the different response in both eigenvalues is due to the component jH_{ol2} in (29). A damping strategy can thus be based on the modification of the cross-coupling between d and q axis. It can also be concluded that DFIG wind turbines connected to series compensated grids can become unstable even if the PLL influence is not considered.

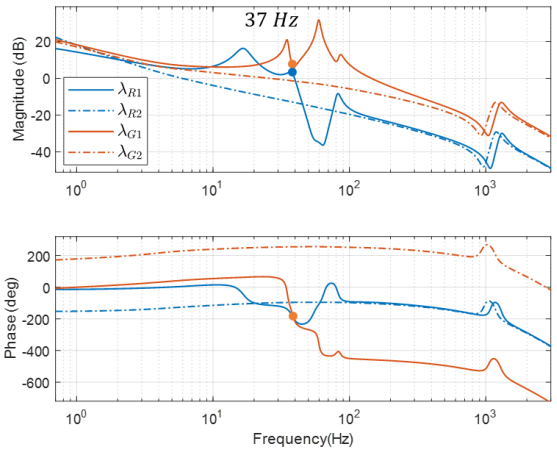

FIGURE 6. Eigenvalues' Bode diagrams for the RSC and GSC current control loops including the PLL.

2) INFLUENCE OF THE PLL ON THE CURRENT CONTROL LOOP STABILITY

The open-loop transfer matrices, $[H_{Gol}]$ and $[H_{Rol}]$, are recalculated for the control loop in Fig. 4, considering the interaction between the GSC and RSC and the PLL. According to (24) and (25), the disturbance introduced by the phase-locked loop depends on the steady-state converter currents and voltages. For the analysis performed in this subsection, both converters are operated at rated power, to increase the disturbance effect [20]. The PLL parameters are provided in Appendix B.

The eigenvalues of the resulting open-loop transfer matrices, $\lambda_{R1,2}$ and $\lambda_{G1,2}$, are computed again, and represented in Fig. 6. It should be noted that the symmetry of $[H_{ol}]$ is broken with the inclusion of the PLL, so the expression for the eigenvalues becomes more complicated. The eigenvalue's Bode diagram including the PLL in Fig. 6 is almost identical to the one presented in Fig. 5 (b). It can be concluded that the PLL used in this paper, with slow dynamics and large stability margins, for the weak grid considered, does not have significant influence on the stability. The SSR instability persist whether the PLL is included or not. In this way, the previous analysis performed without the PLL and the conclusion drawn do not change, and a damping strategy is required to solve the SSR instability. If the wind farm is connected to extremely weak grids, the techniques used in the literature, such as the synchronization with a remote virtual point [33], [34] could be used.

However, as SSRs appear as a result of the interaction between the grid and DFIG impedance, and the GSC and RSC current control loops, in the next section, the influence of the PLL is neglected for simplicity. Thus, the control strategy developed to damp sub-synchronous resonances is proposed and tuned assuming a symmetric MIMO model.

III. SUB-SYNCHRONOUS RESONANCE CONTROL STRATEGY

A. FUNDAMENTALS OF THE SOLUTION

The previous stability analysis demonstrated that the instability is reflected in only one eigenvalue. According to (29),

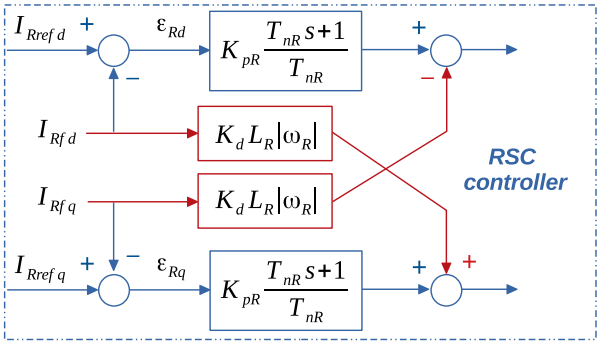

FIGURE 7. Proposed control strategy for the RSC to damp sub-synchronous resonances.

this happens when the cross-coupling terms in the open-loop transfer matrix, H_{ol2}, is different than 0 and in the case under study it even has a greater magnitude than H_{ol1} at some frequencies. For this reason, a sub-synchronous resonance damping strategy can be based on a modification of the cross-couplings between d-q axis, and thus, on the modification of H_{ol2}.

Cross-coupling terms appear in both the GSC and RSC, however, the RSC current control loop parameters have a greater influence on SSRs [7], [10]. The damping strategy is implemented in the RSC current control loop, and is based in already measured local variables, the rotor currents in d-q axis, to avoid the cost of extra sensors in each wind turbine. Fig. 7 represents the proposed control strategy to damp SSR in red. The damping strategy uses the filtered rotor currents and creates an orthogonal proportional voltage action dependent on the absolute value of ω_R, L_R, and a gain, K_d, that is added to the existing PI control action. In Fig. 4 the PI controllers represented are diagonal matrix, so only the orthogonal proportional terms have been added in Fig. 7.

This damping control strategy is implemented in the existing power converter connected to the rotor, the RSC, and does not require additional hardware. It requires low computational burden and can be implemented in the digital signal processor of any power converter. As shown in Fig. 7, it simply requires the addition of an action proportional to the measured rotor currents at the RSC PI output. The action in the d-axis depends on the rotor current in the q-axis and vice-versa.

In the next subsection, the control strategy is adjusted to achieve a robust damping of SSRs for any line compensation level and rotational speeds, two important parameters in the stability of DFIG wind turbines under SSRs.

B. ADJUSTMENT OF THE SSRCS

The proposed sub-synchronous resonance control strategy, based on the rotor current cross-couplings, has a stabilizing effect on the current control loop. In Fig. 8 (a), the RSC and GSC current control open-loop eigenvalues' Bode diagrams have been represented for a $K_d = 3$, a $slip = (\omega_0 - \omega_m)/\omega_0 = 0.25$, and an 80% line impedance compensation level. It can be seen that the proposed control strategy, acting only in the

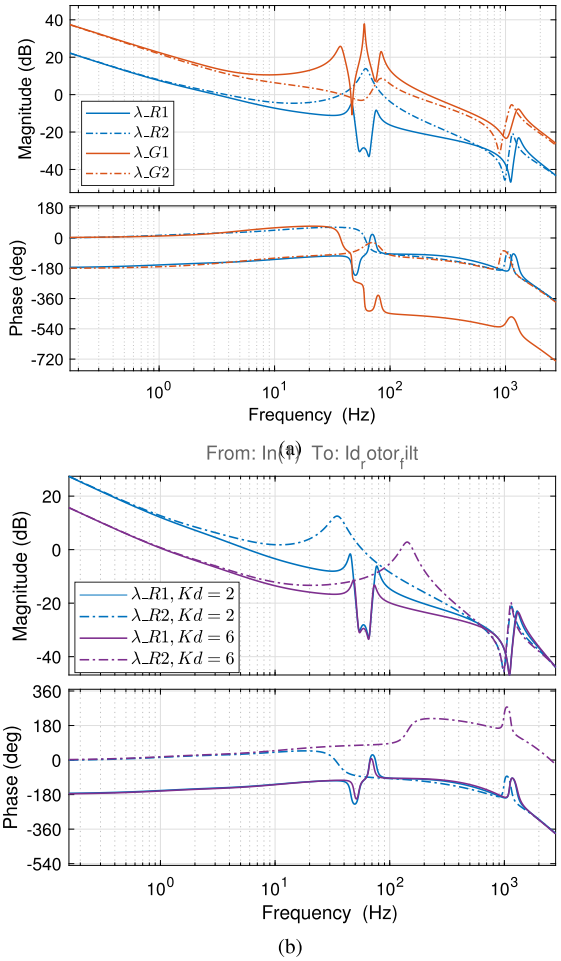

FIGURE 8. Eigenvalues' Bode diagrams for (a) the RSC and GSC current control loops for a $K_d = 3$, and (b) RSC eigenvalues for a $K_d = 2$ and $K_d = 6$.

RSC, can stabilize both the GSC and RSC. The SSRCS introduces a magnitude notch at the SSR in the GSC (compared to Fig. 5 (b)), at a frequency around 45 Hz, avoiding the C^- crossing responsible of the closed-loop instability. In the RSC, the SSRCS reduces the overall magnitude gain, but has a greater effect at the SSR frequency, again, stabilizing the RSC current control loop. It becomes evident from the analysis performed in Fig. 8 (a) that the proposed SSRCS stabilizes the GSC and RSC control loops simultaneously, even though it is only applied in the later. For clarity, in the following, only the RSC eigenvalues are represented to tune the damping strategy.

The influence of the gain K_d on the stability is evaluated in Fig. 8 (b), where the RSC current control open-loop eigenvalues are represented for a $K_d = 2$ and a $K_d = 6$. The SSR appears in λ_{R1}, around 40-50 Hz. It can be seen, that as K_d increases, the magnitude becomes lower, but the resonance peak is decreased even more. However, in the other eigenvalue, λ_{R2}, a greater gain K_d shifts towards higher frequencies a peak in the magnitude plot. It can be seen that for a $K_d = 6$, the current control loop is on the verge of instability at 140 Hz, where a crossing with 180 degrees occur with a magnitude slightly below 0 dB. An increase in K_d will

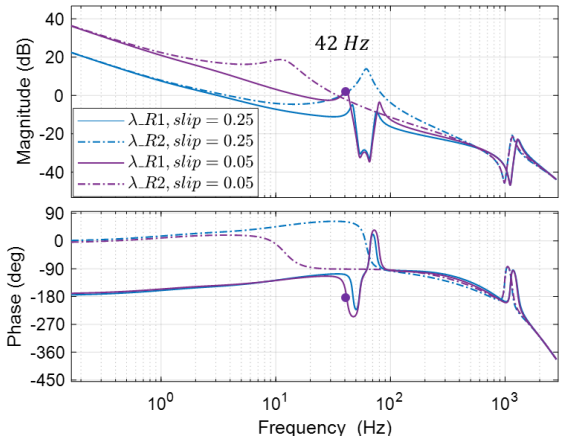

FIGURE 9. Eigenvalues' Bode diagrams for the RSC and GSC current control loops for two different slips at sub-synchronous speed ($K_d = 3$).

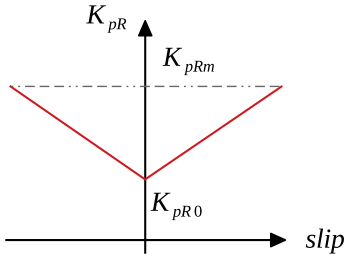

FIGURE 10. Evolution of K_{pR} as a function of the *slip*.

lead to instability. Thus, there is a trade-off in the selection of the SSRCS gain, a greater gain provides larger stability margins at the sub-synchronous resonance frequency, but has a destabilizing effect at higher frequencies.

Another important aspect in DFIG wind turbines is that their dynamics are highly influenced by the rotational speed. Fig. 9 shows how the rotational speed strongly influences the stability of SSRs. The slip equals the ratio $(\omega_0 - \omega_m)/\omega_0$, and it can be concluded that as ω_m approaches ω_0 (as the slip becomes closer to 0), the current control loop changes its dynamics, increasing the magnitude gain. This gain variability creates a problem with SSRs, as in Fig. 9 for a $slip = 0.05$, λ_{R1} has C^- crossing with positive magnitude, and the system becomes unstable. Nevertheless, as the slip is known, this effect can be corrected, and K_{pR} can be modified as a function of the slip.

Taking into account the previous considerations, the proposed SSRCS applies a proportional voltage action in the current control-loop dependent on the cross-currents and modifies the *PI* proportional gain as a function of the slip to mitigate the variability of the system dynamics. The variation of K_{pR} as a function of the slip is represented in Fig.10.

Once the SSRCS has been explained and its influence on the system dynamics characterized, the parameter K_d must be determined, as well as the limits for the variable PI gain; K_{pR0} and K_{pRm}. The design procedure is as follows:

1) Selection of K_d as a trade-off between the stability at the SSR and at higher frequencies.

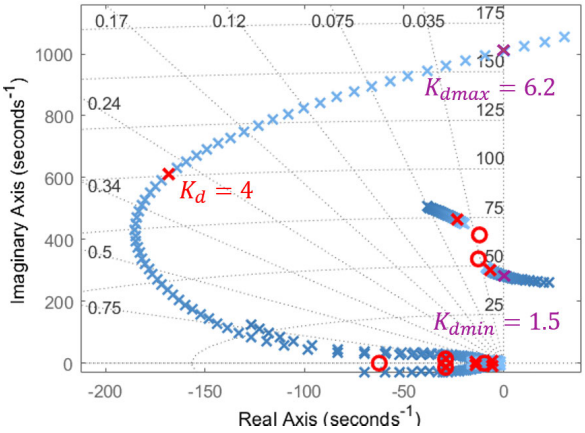

FIGURE 11. Evolution of the poles as a function of the gain K_d.

2) Determination of K_{pR0} and K_{pRm} to achieve a less variable dynamic behavior, once the inner SSRCS is included.

First, the optimal K_d value is selected for a $slip = 0.25$, the lowest possible rotational speed, where SSRs are most likely to occur [1]. To adjust K_d, different proportional gain values are swept to find the optimal one. An analytical adjustment is not a feasible approach, given the high order of the model required to properly capture the system dynamics (order 38). Different K_d values are swept to find the most appropriate gain. In Fig. 11 the evolution of the closed-loop poles is represented as the gain K_d varies from 0 (dark blue poles) to 7 (light blue poles). This figure confirms the results deduced from the Bode diagrams in Fig. 5 (b) and Fig. 8 (b). Without a damping control strategy, the closed-loop system becomes unstable, in fact for $K_d < 1.5$, the system is unstable. As K_d increases, the damping of the SSR poles becomes greater, however, if K_d is increased beyond 6.2, unstable poles at a higher frequency (around 150 Hz) are introduced by the SSRCS. To find a compromise between these two trends, a minimum damping of this higher resonant poles is set equal to 0.25, which leads to $K_d = 4$ (poles in red). With this gain the SSR poles (below 50 Hz) are close to the maximum damping that the proposed strategy can guarantee, while the higher frequency poles are also sufficiently damped. The value of K_d will vary if a different case study with different DFIG wind turbines is considered.

The next step is the adjustment of K_{pR0} and K_{pRm}. Both parameters are determined with the purpose of having an almost constant cutoff frequency for every rotational speed. If the RSC current control loop cut-off frequency is set to 10 Hz and is kept constant for every rotational speed, $K_{pR0} = 0.02$ and $K_{pRm} = 0.14$.

C. SSRCS ROBUSTNESS ANALYSIS

Finally, the robustness of the proposed SSRCS is evaluated for several line impedance compensation levels in Fig. 12: (a) 0%, (b) 20%, (c) 50% and (d) 80%. The SSRCS is adjusted as described in the previous section, with $K_d = 4$. For each line impedance compensation level, the wind speed is

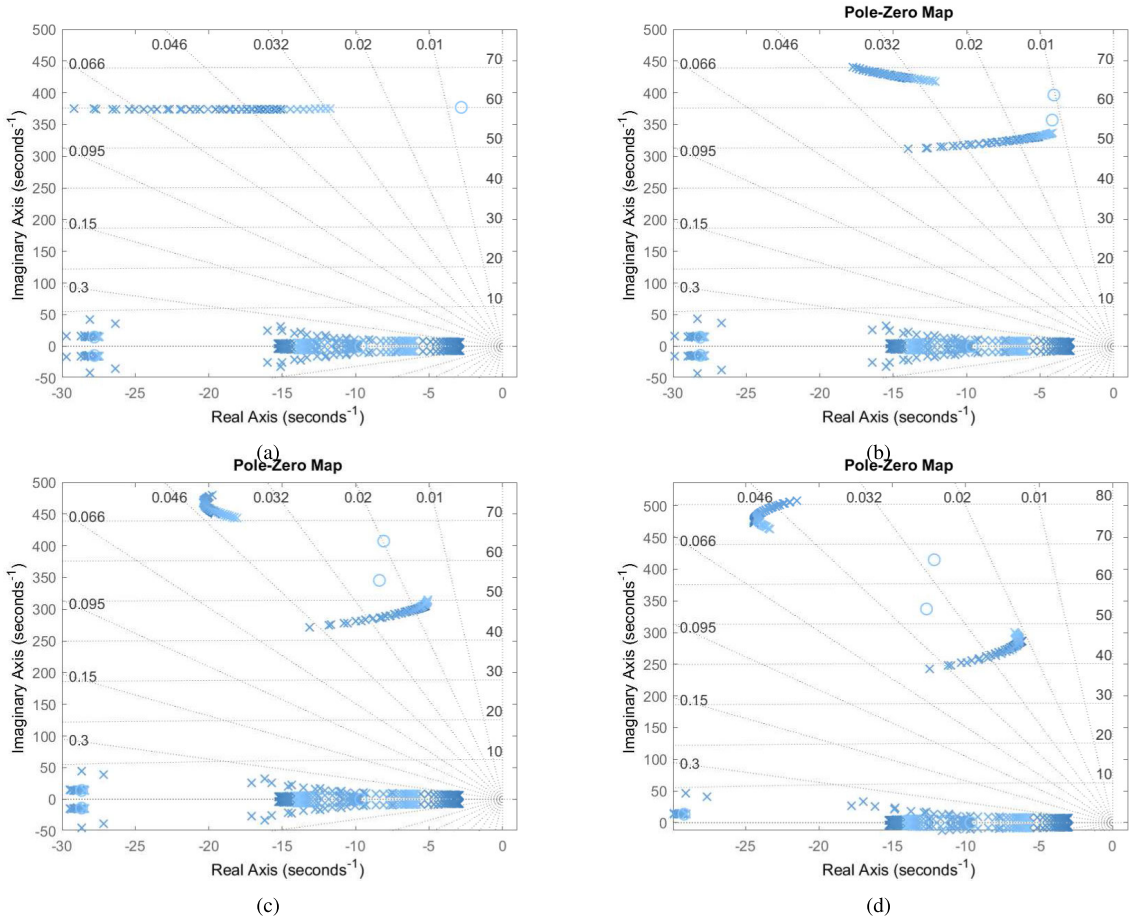

FIGURE 12. Closed-loop poles for different slips ($-0.25 < slip < 0.25$) and four line impedance compensation levels: (a) 0%, (b) 20%, (c) 50% and (d) 80%.

varied starting at the cut-in speed up to the cut-out speed. This way, the rotational mechanical speed is varied from the minimal value, $slip = 0.25$, to its maximum value, $slip = -0.25$. The model used for the robustness analysis includes the PLL. For every line impedance compensation level, the system closed-loop poles are represented, and as the rotational speed increases, the poles are depicted in lighter blue color. It can be seen that the proposed control strategy is able to stabilize the system for any line impedance compensation level and rotational speed (wind speed), proving to be robust.

IV. VALIDATION OF THE CONTROL STRATEGY

To validate the proposed model for the DFIG wind turbine and the sub-synchronous resonance damping control strategy, a model of a 2 MW DFIG wind turbine is built in MATLAB/Simulink with the components from the Simscape Electrical Library. The system parameters for the DFIG wind turbines and the transmission line are specified in Appendix B.

A. MODEL VALIDATION

First of all, the linearized model developed previously, using transfer function matrices, is validated with the Simulink model. The model developed in MATLAB/Simulink includes the PLL, the active and reactive power control loops as well as the current reference computations. Moreover, it also includes non-linear elements such as the converter IGBTs and the space vector pulse-width modulation.

To validate the model for the DFIG wind turbine developed in this paper the current step response of the analytical model is compared to the current step response of the MATLAB/Simulink model for two different slips, a $slip = 0.25$ and -0.2. A 1 MW step is introduced in the grid by the RSC and the GSC to validate both responses.

Fig. 13 shows the simulation results for an 80% line impedance compensation level. There is an agreement between both models, that exhibit almost identical current step responses. The main difference is the switching ripple present in the Simulink model. In this figure, the subscript S stands for Simulink, while m stands for the matrix impedance model. These simulation results validate the proposed model and modeling methodology for DFIG wind turbines. Moreover, it proves that the novel SSRCS presented in this paper, with $K_d = 4$ and the variable K_{pR}, can effectively stabilize the system for an 80% line compensation level and different rotational speeds, a conclusion that agrees with the results derived from the stability analysis and represented in Fig. 11 and 12.

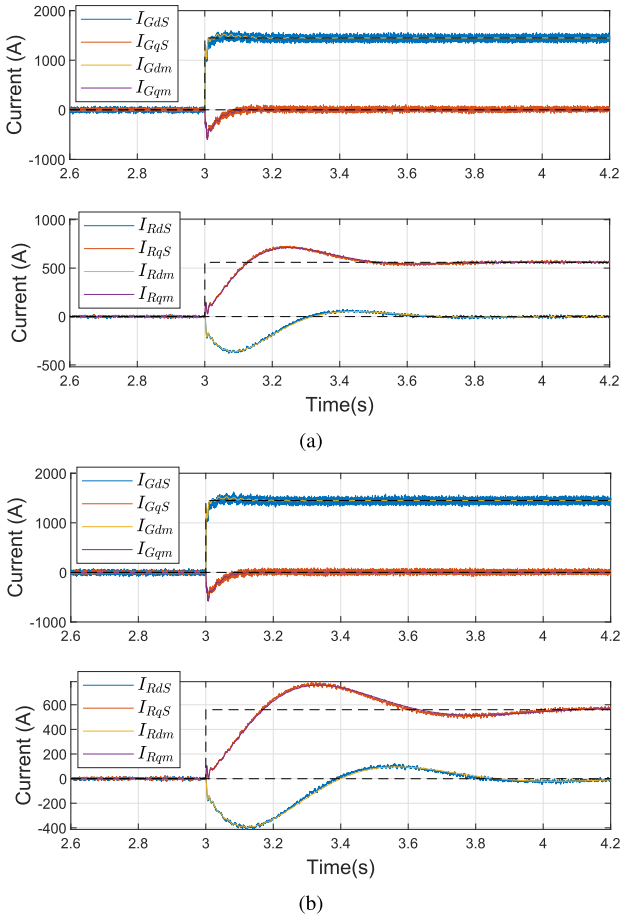

FIGURE 13. Current controller step response comparison for an 80% line compensation level and two different DFIG slips (a) *slip* = 0.25, and (b) *slip* = −0.2.

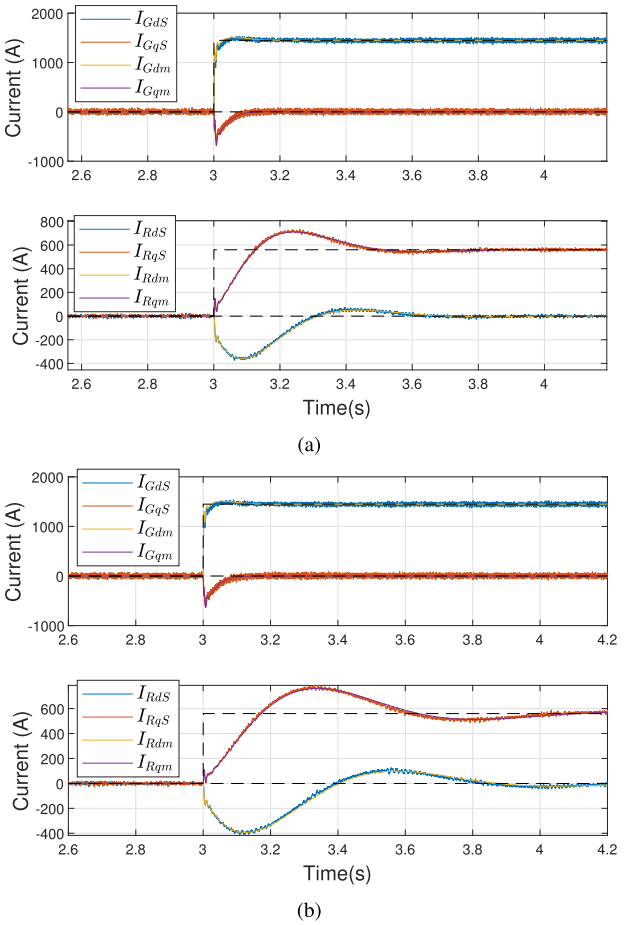

FIGURE 14. Current controller step response comparison for a 20% line compensation level and two different DFIG slips (a) *slip* = 0.25, and (b) *slip* = −0.2.

The same simulation is repeated for a 20% line compensation level and the same rotational speeds, the results are represented in Fig. 14. Again, both models present a perfect agreement and thus the matrix impedance model developed and the stability shown in Fig. 12 (b) are validated. It can be seen that for a 20% line impedance compensation level, the switching ripple is lower, as the grid is more inductive.

Both simulations prove as well that the proposed control strategy proposed for the RSC can effectively damp sub-synchronous resonance oscillations, as the system has a stable response in both cases.

B. SUB-SYNCHRONOUS RESONANCE DAMPING STRATEGY VALIDATION

To validate the performance of the proposed control strategy for the RSC, a simulation is performed where the line impedance compensation level is transiently modified, starting at 80%, reduced to 50% and at last with no line compensation. The simulation has been performed for a slip equal to 0.25.

In Fig. 15 the line series capacitor voltage, the line active power and line currents are represented. The figure proves that the proposed SSRCS is able to perfectly damp sub-synchronous resonances, regardless of the line

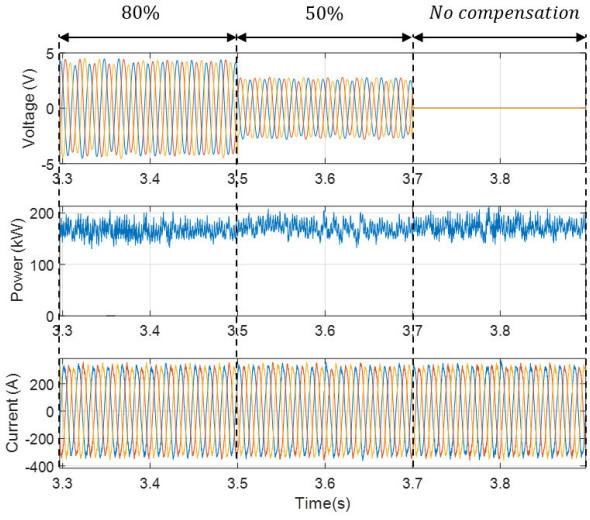

FIGURE 15. Simulation performed for a *slip* = 0.25 and three different line impedance compensation levels.

impedance compensation level, a result that agrees with the pole diagrams represented in Fig. 12.

In the stability analysis it was also demonstrated that the DFIG wind turbine was unstable when connected to a series compensated transmission line, with a compensation level

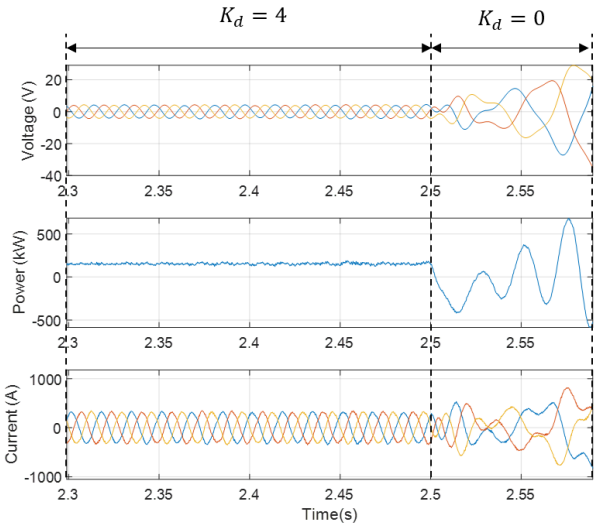

FIGURE 16. Simulation performed for a *slip* = 0.25 and an 80% compensation level, transiently disabling the SSRCS.

equal to 80% and a *slip* = 0.25. As concluded from Fig. 5, the interaction between the GSC and the RSC has to be modeled and studied, as otherwise such instability is not captured. In order to validate this analysis, the DFIG wind turbine is connected to the grid with the SSRCS adjusted in this paper enabled, and it is disabled when the simulation time reaches 2.5 s. The same variables as in Fig. 15 are represented: the line series capacitor voltage, the line active power and line currents. It becomes evident from Fig. 16 that the system without a damping strategy becomes unstable, and that both the GSC and RSC and its interaction have to be modeled to properly characterize the phenomena.

C. LARGE DISTURBANCE PERFORMANCE

Large disturbances can trigger sub-synchronous resonances, for this reason, in this subsection the proposed damping strategy is tested when a voltage sag occurs in the grid.

To simulate this circumstance, a three-phase-to-ground fault on the series compensated line is forced at 2.5 s. The simulation results are represented in Fig. 17 for two line impedance compensation levels, an 80% in Fig. 17 (a) and a 20% in Fig. 17 (b). In both cases, the DFIG wind turbine is stable and SSRs are properly damped, as demonstrated by the RSC and GSC current waveform.

The validation section confirms that the SSRCS can effectively damp sub-synchronous resonances for different operation conditions, proving to be robust.

V. CONCLUSION

DFIG wind turbines connected to capacitive series-compensated transmission lines are prone to SSR instability. To characterize the system dynamics and the causes of instability, a model in the *d-q* reference frame is developed in this paper based on 2×2 impedance matrices. A systematic modeling approach is presented for DFIG wind turbines, where different reference frames exist, and thus, the transformation

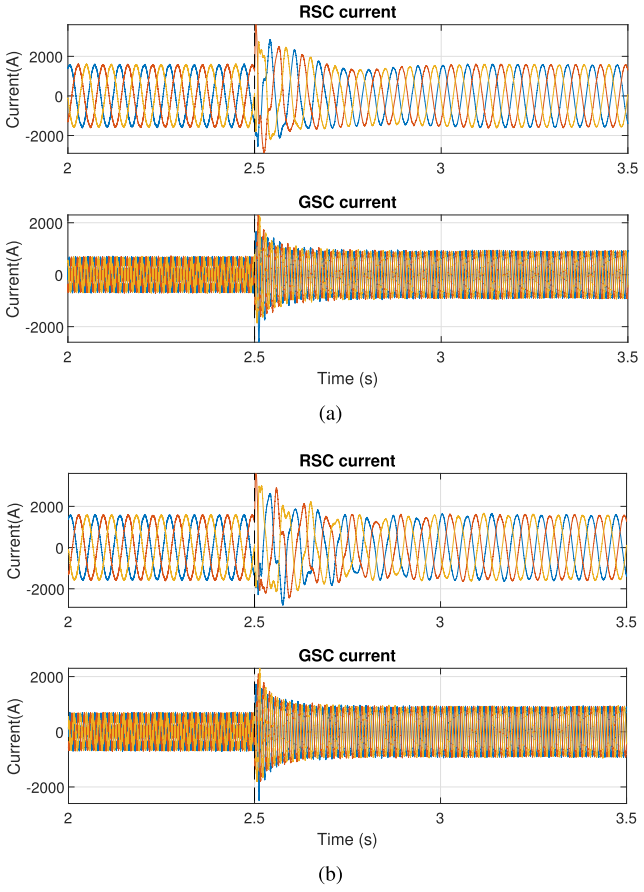

FIGURE 17. RSC and GSC current when a three-phase-to-ground fault occurs in the transmission line for two line impedance compensation levels: (a) 80%, and (b) 20%.

of the component models between these reference frames becomes specially important. The system stability is analyzed by means of the open-loop matrix eigenvalue Bode diagram, a more intuitive tool to design controllers for power electronic engineers than the closed-loop eigenvalues commonly used to analyze SSRs. Through this stability analysis, we identify that the interaction between the RSC and GSC control loops are a source of instability in DFIG wind turbines connected to series-compensated grids. It becomes evident that DFIG WECS need a sub-synchronous resonance damping control strategy (SSRCS) when connected to series compensated transmission lines. For this reason, a novel control strategy is presented that uses the DFIG rotor current and is implemented in the existing power converter connected to the rotor. Thus, as it is based in already measured variables and implemented in the existing RSC, it does not imply an extra cost and can be applied to any new or existing wind turbine. Moreover, the SSRCS requires minimal modifications of the control loops. The SSRCS is based on a proportional action dependent of the rotor cross-currents obtained in *d-q* coordinates. The strategy also implements a variable PI gain dependent on the rotor speed. Both the theoretical analysis and the simulation results for a real case study demonstrate that the proposed control strategy for the RSC is able to damp sub-synchronous resonances and stabilize a wind farm

TABLE 2. System Parameters.

Parameter	Magnitude
Distribution grid (Zorillo-Rio Hondo) $S_B = 100\ MVA, U = 345\ kV$	
Line reactance	0.034 p.u.
Line resistance	0.003 p.u.
Wind farm substation $S_B = 250\ MVA, 34.5/345\ kV$	
Reactance	0.1 p.u.
Resistance	0.004 p.u.
Wind farm grid $S_B = 100\ MVA, U = 34.5\ kV$	
Line reactance	0.013 p.u.
Line resistance	0.008 p.u.
Wind turbine transformer $S_B = 2.5\ MVA, 34.5/0.69\ kV$	
Reactance	0.05 p.u.
Resistance	0.007 p.u.
DFIG $S_B = 2.5\ MVA, U = 690\ V$	
Number of turbines	100
Rotor resistance	0.008 p.u.
Rotor leakage inductance	0.102 p.u.
Stator resistance	0.006 p.u.
Stator leakage inductance	0.097 p.u.
Magnetizing inductance	4.34 p.u.
Power converter	
Rated power	500 *kVA*
Switching frequency	2.8 kHz
Sampling frequency	5.6 kHz
GSC reactance	0.2 p.u.
GSC resistance	0.005 p.u.
GSC filter capacitor	0.036 p.u.
GSC filter series damping resistance	0.21 p.u.
Control parameters	
GSC PI proportional gain	0.1
GSC PI integral constant	0.03
RSC PI proportional gain	See Fig. 10
RSC PI integral constant	0.016
Low-pass analog filter time constant	20.10^{-6}
PLL PI proportional gain	0.2
PLL PI integral constant	0.22
SOGI proportional gain	0.2

for any line impedance compensation level and wind turbine operation point, and does not require real-time information regarding the grid impedance and series compensation level, proving to be an effective and robust strategy.

APPENDIX A
PLANT MODEL

$$[P_{I_G V_G}] = \left([I_2] + [Z_{RL_G}]_{\omega_0}^{-1} \left([Z_g]_{\omega_0}^{-1} + [Z_{Cf}]_{\omega_0}^{-1} + [Y_{I_S V_S}]\right)^{-1}\right) [Z_{RL_G}]_{\omega_0}^{-1} \tag{30}$$

$$[P_{I_G V_R}] = \left([I_2] + [Z_{RL_G}]_{\omega_0}^{-1} \left([Z_g]_{\omega_0}^{-1} + [Y_{I_S V_S}] + [Z_{Cf}]_{\omega_0}^{-1}\right)\right)^{-1} [Z_{RL_G}]_{\omega_0}^{-1} \left([Z_g]_{\omega_0}^{-1} + [Y_{I_S V_S}] + [Z_{Cf}]_{\omega_0}^{-1}\right)^{-1} [Y_{I_S V_R}] \tag{31}$$

$$[P_{I_R V_G}] = [Y_{I_R V_S}] \left([I_2] + [Z_{Cf}]_{\omega_0} \left([Z_g]_{\omega_0}^{-1} + [Y_{I_S V_S}] + [Z_{RL_G}]_{\omega_0}^{-1}\right)\right)^{-1} [Z_{Cf}]_{\omega_0} [Z_{RL_G}]_{\omega_0}^{-1} \tag{32}$$

$$[P_{I_R V_R}] = -[Y_{I_R V_R}] - [Y_{I_R V_S}] \left([I_2] + [Z_{Cf}]_{\omega_0} \left([Z_g]_{\omega_0}^{-1} + [Z_{RL_G}]_{\omega_0}^{-1} + [Y_{I_S V_S}]\right)\right)^{-1} [Z_{Cf}]_{\omega_0} [Y_{I_S V_R}] \tag{33}$$

APPENDIX B
SYSTEM PARAMETERS

See Table 2.

REFERENCES

[1] L. Fan, R. Kavasseri, Z. L. Miao, and C. Zhu, "Modeling of DFIG-based wind farms for SSR analysis," *IEEE Trans. Power Del.*, vol. 25, no. 4, pp. 2073–2082, Oct. 2010.

[2] E. V. Larsen, "Wind generators and series-compensated AC transmission lines," in *Proc. IEEE Power Energy Soc. Gen. Meeting*, May 2012, pp. 1–4.

[3] J. Daniel, C. Han, S. Hutchinson, R. Koessler, D. Martin, G. Shen, and W. Wong, "Ercot crez reactive power compensation study," ABB Inc., Power Syst. Division, Grid Syst. Consulting, Raleigh, NC, USA, Tech. Rep. E3800-PR-00, 2010.

[4] M. Bongiorno, A. Petersson, and E. Agneholm, "The impact of wind farms on subsynchronous resonance in power systems," ELFORSK, Copenhague, Denmark, Elforsk Rep. 11:29, 2011, p. 29, vol. 11.

[5] K. Narendra, D. Fedirchuk, R. Midence, N. Zhang, A. Mulawarman, P. Mysore, and V. Sood, "New microprocessor based relay to monitor and protect power systems against sub-harmonics," in *Proc. IEEE Electr. Power Energy Conf.*, Oct. 2011, pp. 438–443.

[6] L. Wang, X. Xie, Q. Jiang, H. Liu, Y. Li, and H. Liu, "Investigation of SSR in practical DFIG-based wind farms connected to a series-compensated power system," *IEEE Trans. Power Syst.*, vol. 30, no. 5, pp. 2772–2779, Sep. 2015.

[7] L. Fan and Z. Miao, "Mitigating SSR using DFIG-based wind generation," *IEEE Trans. Sustain. Energy*, vol. 3, no. 3, pp. 349–358, Jul. 2012.

[8] H. A. Mohammadpour and E. Santi, "Sub-synchronous resonance analysis in DFIG-based wind farms: Definitions and problem identification—Part I," in *Proc. IEEE Energy Convers. Congr. Expo. (ECCE)*, Sep. 2014, pp. 812–819.

[9] H. A. Mohammadpour and E. Santi, "Sub-synchronous resonance analysis in DFIG-based wind farms: Mitigation methods—TCSC, GCSC, and DFIG controllers—Part II," in *Proc. IEEE Energy Convers. Congr. Expo. (ECCE)*, Sep. 2014, pp. 1550–1557.

[10] H. A. Mohammadpour and E. Santi, "SSR damping controller design and optimal placement in rotor-side and grid-side converters of series-compensated DFIG-based wind farm," *IEEE Trans. Sustain. Energy*, vol. 6, no. 2, pp. 388–399, Apr. 2015.

[11] A. E. Leon and J. A. Solsona, "Sub-synchronous interaction damping control for DFIG wind turbines," *IEEE Trans. Power Syst.*, vol. 30, no. 1, pp. 419–428, Jan. 2015.

[12] P.-H. Huang, M. S. El Moursi, W. Xiao, and J. L. Kirtley, "Subsynchronous resonance mitigation for series-compensated DFIG-based wind farm by using two-degree-of-freedom control strategy," *IEEE Trans. Power Syst.*, vol. 30, no. 3, pp. 1442–1454, May 2015.

[13] A. E. Leon, "Integration of DFIG-based wind farms into series-compensated transmission systems," *IEEE Trans. Sustain. Energy*, vol. 7, no. 2, pp. 451–460, Apr. 2016.

[14] L. Fan and Z. Miao, "Nyquist-stability-criterion-based SSR explanation for type-3 wind generators," *IEEE Trans. Energy Convers.*, vol. 27, no. 3, pp. 807–809, Sep. 2012.

[15] I. Vieto and J. Sun, "Sequence impedance modeling and analysis of type-III wind turbines," *IEEE Trans. Energy Convers.*, vol. 33, no. 2, pp. 537–545, Jun. 2018.

[16] Z. Miao, "Impedance-model-based SSR analysis for type 3 wind generator and series-compensated network," *IEEE Trans. Energy Convers.*, vol. 27, no. 4, pp. 984–991, Dec. 2012.

[17] H. J. Baesmat and M. Bodson, "Suppression of sub-synchronous resonances through excitation control of doubly fed induction generators," *IEEE Trans. Power Syst.*, vol. 34, no. 6, pp. 4329–4340, Nov. 2019.

[18] X. Zhang, Y. Zhang, R. Fang, and D. Xu, "Impedance modeling and SSR analysis of DFIG using complex vector theory," *IEEE Access*, vol. 7, pp. 155860–155870, 2019.

[19] D. N. Zmood, D. G. Holmes, and G. H. Bode, "Frequency-domain analysis of three-phase linear current regulators," *IEEE Trans. Ind. Appl.*, vol. 37, no. 2, pp. 601–610, Oct. 2001.

[20] B. Wen, D. Boroyevich, R. Burgos, P. Mattavelli, and Z. Shen, "Analysis of D-Q small-signal impedance of grid-tied inverters," *IEEE Trans. Power Electron.*, vol. 31, no. 1, pp. 675–687, Jan. 2016.

[21] A. Rygg, M. Molinas, C. Zhang, and X. Cai, "A modified sequence-domain impedance definition and its equivalence to the dq-domain impedance definition for the stability analysis of AC power electronic systems," *IEEE J. Emerg. Sel. Topics Power Electron.*, vol. 4, no. 4, pp. 1383–1396, Dec. 2016.

[22] J. Samanes, A. Urtasun, E. Gubia, and A. Petri, "Robust multisampled capacitor voltage active damping for grid-connected power converters," *Int. J. Electr. Power Energy Syst.*, vol. 105, pp. 741–752, Feb. 2019.
[23] J. Samanes, A. Urtasun, E. L. Barrios, D. Lumbreras, J. Lopez, E. Gubia, and P. Sanchis, "Control design and stability analysis of power converters: The MIMO generalized bode criterion," *IEEE J. Emerg. Sel. Topics Power Electron.*, vol. 8, no. 2, pp. 1880–1893, Jun. 2020.
[24] R. K. Varma, S. Auddy, and Y. Semsedini, "Mitigation of subsynchronous resonance in a series-compensated wind farm using FACTS controllers," *IEEE Trans. Power Del.*, vol. 23, no. 3, pp. 1645–1654, Jul. 2008.
[25] M. S. El-Moursi, B. Bak-Jensen, and M. H. Abdel-Rahman, "Novel STATCOM controller for mitigating SSR and damping power system oscillations in a series compensated wind park," *IEEE Trans. Power Electron.*, vol. 25, no. 2, pp. 429–441, Feb. 2010.
[26] T. Joseph, C. E. Ugalde-Loo, S. Balasubramaniam, J. Liang, and G. Li, "Experimental validation of an active wideband SSR damping scheme for series-compensated networks," *IEEE Trans. Power Del.*, vol. 35, no. 1, pp. 58–70, Feb. 2020.
[27] H. Liu, X. Xie, Y. Li, H. Liu, and Y. Hu, "Mitigation of SSR by embedding subsynchronous notch filters into DFIG converter controllers," *IET Gener., Transmiss. Distrib.*, vol. 11, no. 11, pp. 2888–2896, Aug. 2017.
[28] J. Samanes, L. Rosado, E. Gubia, and J. Lopez, "Sub-synchronous resonance damper based on the stator voltage feedback for DFIG wind turbines," in *Proc. IEEE 21st Workshop Control Modeling Power Electron. (COMPEL)*, Nov. 2020, pp. 671–678.
[29] J. L. Agorreta, M. Borrega, J. López, and L. Marroyo, "Modeling and control of *N*-paralleled grid-connected inverters with LCL filter coupled due to grid impedance in PV plants," *IEEE Trans. Power Electron.*, vol. 26, no. 3, pp. 770–785, Mar. 2011.
[30] X. Wang, L. Harnefors, and F. Blaabjerg, "Unified impedance model of grid-connected voltage-source converters," *IEEE Trans. Power Electron.*, vol. 33, no. 2, pp. 1775–1787, Feb. 2018.
[31] M. Xie, H. Wen, C. Zhu, and Y. Yang, "DC offset rejection improvement in single-phase SOGI-PLL algorithms: Methods review and experimental evaluation," *IEEE Access*, vol. 5, pp. 12810–12819, 2017.
[32] Z. Xie, Y. Chen, W. Wu, Y. Xu, H. Wang, J. Guo, and A. Luo, "Modeling and control parameters design for grid-connected inverter system considering the effect of PLL and grid impedance," *IEEE Access*, vol. 8, pp. 40474–40484, 2020.
[33] W. Cao, Y. Ma, J. Wang, and F. Wang, "Virtual series impedance emulation control for remote PV or wind farms," in *Proc. IEEE Appl. Power Electron. Conf. Expo. (APEC)*, Mar. 2014, pp. 411–418.
[34] J. A. Suul, S. D'Arco, P. Rodríguez, and M. Molinas, "Impedance-compensated grid synchronisation for extending the stability range of weak grids with voltage source converters," *IET Gener., Transmiss. Distrib.*, vol. 10, no. 6, pp. 1315–1326, Apr. 2016.

JAVIER SAMANES (Member, IEEE) was born in Pamplona, Spain, in 1990. He received the M.Sc. degree in electrical engineering, the M.Sc. degree in renewable energy engineering, and the Ph.D. degree in electrical engineering from the Public University of Navarre (UPNA), Pamplona, in 2014, 2016, and 2018, respectively.

In 2014, he joined the Electrical Engineering, Power Electronics and Renewable Energy Research Group (INGEPER), UPNA, where he is currently an Assistant Professor and a member of the Institute of Smart Cities (ISC). In 2018, he was a Visiting Scholar with the Center for Power Electronic Systems (CPES), Virginia Tech, USA. His research interests include power electronics and renewable energies.

EUGENIO GUBIA (Member, IEEE) received the M.Sc. and Ph.D. degrees in industrial engineering from the Public University of Navarre, Spain, in 1995 and 2003, respectively.

He joined the Electrical and Electronic Department, Public University of Navarre, in 1996, where he is currently an Associate Professor and a member of the Institute of Smart Cities (ISC). In 2002, he joined the Electrical Engineering, Power Electronics, and Renewable Energy Research Group (INGEPER). From June to December 2005, he worked as a Guest Researcher with the Center for Power Electronics Systems (CPES) in the field of electromagnetic compatibility. His research interests include power electronics, renewable energy systems, high-frequency phenomena, and electromagnetic compatibility.

JESUS LOPEZ (Member, IEEE) was born in Pamplona, Spain, in 1975. He received the M.Sc. degree in industrial engineering from the Public University of Navarra, Pamplona, in 2000, and the Ph.D. degree in industrial engineering from the Public University of Navarra, in collaboration with the LAPLACE laboratory, Toulouse, France, in 2008.

In 2001, he joined the Power Electronic Group, Electrical and Electronic Department, Public University of Navarra, where he is currently an Assistant Professor and is also involved in research projects mainly in co-operation with industry. His research interests include power electronics, power systems quality, and renewable energies, such as wind turbines and photovoltaic plants.

ROLANDO BURGOS (Member, IEEE) received the B.S. degree in electronics engineering, the Electronics Engineering Professional degree, and the M.S. and Ph.D. degrees in electrical engineering from the University of Concepción, Chile, in 1995, 1997, 1999, and 2002, respectively.

In 2002, he joined, as a Postdoctoral Fellow, the Center for Power Electronics Systems (CPES), Virginia Tech, Blacksburg, VA, USA, becoming as a Research Scientist, in 2003, and a Research Assistant Professor, in 2005. In 2009, he joined ABB Corporate Research, Raleigh, NC, USA, where he was a Scientist from 2009 to 2010, and a Principal Scientist from 2010 to 2012. In 2010, he was appointed as an Adjunct Associate Professor with the Electrical and Computer Engineering Department, North Carolina State University, and with the Future Renewable Electric Energy Delivery and Management (FREEDM) Systems Center. In 2012, he returned to Virginia Tech as an Associate Professor with The Bradley Department of Electrical and Computer Engineering, where he was promoted to a Professor in 2019. His research interests include high power density wide-bandgap semiconductor-based power conversion—low voltage and medium voltage applications, packaging and integration, electromagnetic interference (EMI) and electromagnetic compatibility (EMC), multi-phase multi-level power converters, modeling and control, grid power electronics systems, and the stability of ac and dc power systems. He is a member of the IEEE Industry Applications Society, the IEEE Industrial Electronics Society, and the IEEE Power and Energy Society. He is also a member of the IEEE Power Electronics Society, where he serves the Chair for the Technical Committee on Power and Control Core Technologies. He also serves as an Associate Editor for the IEEE TRANSACTIONS ON POWER ELECTRONICS, and the IEEE JOURNAL OF EMERGING AND SELECTED TOPICS IN POWER ELECTRONICS.